THE JOURNAL OF PHYSICAL CHEMISTRY A
A JOURNAL OF THE AMERICAN CHEMICAL SOCIETY

pubs.acs.org/JPCA
Article

Electronic Structure of the Complete Series of Gas-Phase Manganese Acetylacetonates by X-ray Absorption Spectroscopy

Olesya S. Ablyasova, Meiyuan Guo, Vicente Zamudio-Bayer, Markus Kubin, Tim Gitzinger, Mayara da Silva Santos, Max Flach, Martin Timm, Marcus Lundberg, J. Tobias Lau, and Konstantin Hirsch*

Cite This: J. Phys. Chem. A 2023, 127, 7121−7131
Read Online

ABSTRACT: Metal centers in transition metal−ligand complexes occur in a variety of oxidation states causing their redox activity and therefore making them relevant for applications in physics and chemistry. The electronic state of these complexes can be studied by X-ray absorption spectroscopy, which is, however, due to the complex spectral signature not always straightforward. Here, we study the electronic structure of gas-phase cationic manganese acetylacetonate complexes $Mn(acac)^{+}_{1-3}$ using X-ray absorption spectroscopy at the metal center and ligand constituents. The spectra are well reproduced by multiconfigurational wave function theory, time-dependent density functional theory as well as parameterized crystal field and charge transfer multiplet simulations. This enables us to get detailed insights into the electronic structure of ground-state $Mn(acac)^{+}_{1-3}$ and extract empirical parameters such as crystal field strength and exchange coupling from X-ray excitation at both the metal and ligand sites. By comparison to X-ray absorption spectra of neutral, solvated $Mn(acac)_{2,3}$ complexes, we also show that the effect of coordination on the L_3 excitation energy, routinely used to identify oxidation states, can contribute about 40−50% to the observed shift, which for the current study is 1.9 eV per oxidation state.

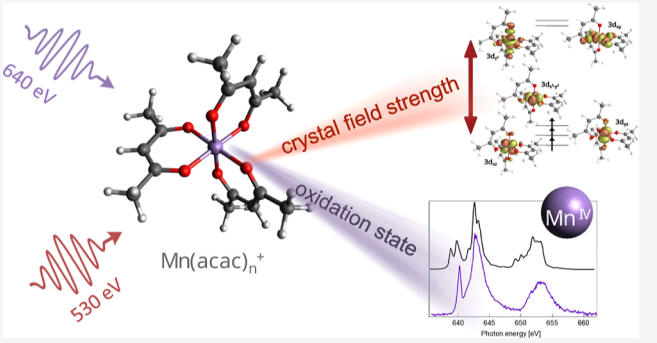

INTRODUCTION

There is a longstanding interest in transition-metal acetylacetonate (acac) complexes that has been renewed in recent years due to promising applications in redox flow batteries,[1,2] industrial aqueous synthesis of metal−organic-frameworks,[3] and as possible single-molecule magnets[4] even showing spin crossover behavior in related transition-metal complexes.[5] Furthermore, transition-metal complexes are relevant for catalysis[6,7] while the attractiveness of transition-metal acetylonates in particular is based on the ability to chemically control their redox activity by coordination or de-coordination of the metal center.[8] Among the 3d transition metals, manganese is well known as the main driver of the catalytic water splitting reaction mediated by the oxygen-evolving complex[9−13] and is relevant as a catalyst in other chemical synthesis reactions as it has access to a variety of oxidation states ranging from −3 to +7.[14−16] Thus, via the interplay of coordination and oxidation states of the manganese atom the properties of manganese acetylacetonate complexes can be tailored and controlled.

The neutral $Mn(acac)_{2,3}$ molecules in solution were successfully investigated earlier,[17−19] but the singly coordinated $Mn(acac)_1$ has never been observed in solution. Here, we show that the low-coordinated $Mn(acac)^{+}_1$ complex can be accessed in the gas phase. We are therefore able to investigate the complete range of coordination of cationic $Mn(acac)^{+}_n$, n = 1−3 using X-ray absorption spectroscopy (XAS). By employing XAS to the metal center and the ligand we obtain complementary information on the electronic structure of the system.[20,21] We also perform time-dependent density functional theory (TD-DFT) calculations at the oxygen and carbon K-edges and restricted active space (RAS) calculations accompanied by charge transfer multiplet (CTM) simulations at the manganese $L_{2,3}$ edges. This enables us to get an in-depth insight into the electronic structure of $Mn(acac)^{+}_n$, n = 1−3.

METHODS

Experimental Details. Experiments were performed at the Ion Trap endstation[22,23] at beamline UE52 PGM of the synchrotron radiation facility BESSY II operated by the Helmholtz-Zentrum Berlin. Electrospraying-solvated Mn-

Received: April 28, 2023
Revised: July 28, 2023
Published: August 17, 2023

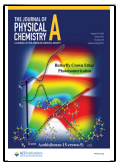

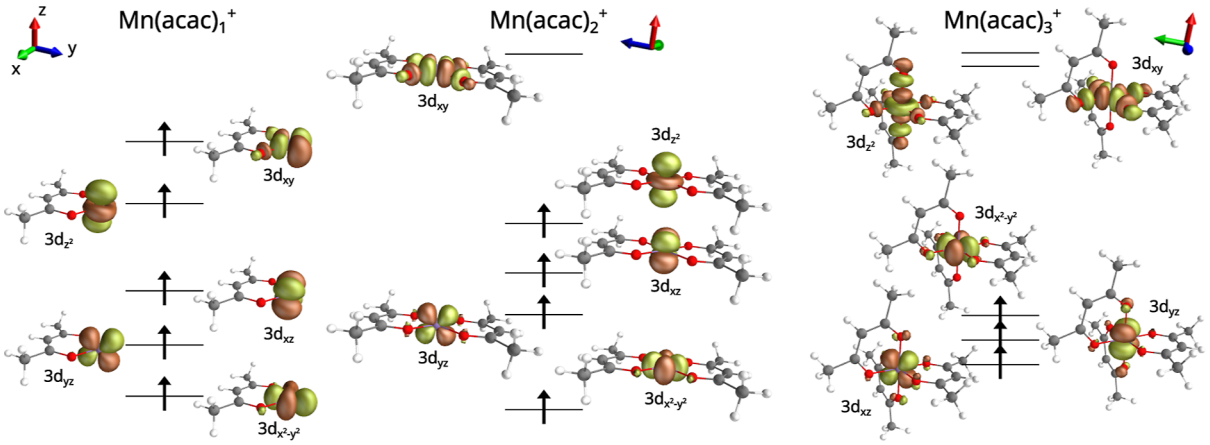

Figure 1. Ground-state structures of $Mn(acac)^{+}_{1-3}$ complexes. Additionally shown are isosurface plots of the RAS valence orbitals. Occupied orbitals are indicated by an ↑.

$(acac)_3$ molecules generates gas-phase cationic $Mn(acac)^{+}_{1-3}$ by successive removal of the acetylacetonate ligands depending on spray conditions and ion funnel settings. Two solutions were prepared using 1 mg (560 μg) of $Mn^{III}(acac)_3$ solvated in 5 mL (6.65 mL) acetonitrile resulting in a concentration of 0.57 mM (0.24 mM) both giving the same results. The molecule of interest is accumulated in a liquid helium-cooled linear Paul trap after selection using a quadrupole mass filter. The mass spectrum of selected $Mn(acac)^{+}_{n}$ complexes, n = 1−3, is shown in Supporting Information, Figure S8. A monochromatic X-ray beam excites the sample along the trap axis. X-ray absorption by the ions is followed by an Auger cascade leading to dissociation of the molecule due to Coulomb explosion. X-ray absorption is measured in ion yield mode by detecting photo fragments (listed in Supporting Information, Table S4) using a time-of-flight mass spectrometer. Energy resolution and step size at the different absorption edges are given in Supporting Information, Table S2. Photon energy calibration was performed using neon K-edge photoionization in the beamline ionization cell[24] and checked at the oxygen K-edge, giving a photon energy uncertainty of ±0.1 eV.

Computational Details. Geometry optimization of all complexes was performed with Gaussian 09. E01,[25] using DFT employing the B3LYP functional[26,27] and 6-31G(d) basis set.[28] Cartesian coordinates of all ground-state structures are given in the Supporting Information. For $Mn(acac)^{+}_{2}$, two structures, a planar and a distorted square planar, appeared close in energy. For these two structures, relative stabilities were calculated with B3LYP/6-311+G(2df,2pd)[28] as well as CASPT2[29]/ANO-RCC-VTZP.[30] The CASPT2 calculations were performed with OpenMolcas v18.09.[31]

The carbon and oxygen K-edge XAS were calculated with the ORCA 4.1.2 software package using TD-DFT and employing B3LYP/6-31G(d) functional and basis set. The calculated spectra were broadened with Gaussian functions with FWHM = 0.6 eV and shifted in energy as listed in Supporting Information, Table S3 for carbon K-edge and oxygen K-edge XAS to match the energies of the experimental spectra.

The manganese $L_{2,3}$ edge XA spectra were calculated using the RAS approach[32−34] in OpenMOLCAS v18.09 with RASPT2[35]/ANO-RCC-VDZP using a minimal active space of five metal 3d character orbitals. These orbitals were placed in the RAS2 space where all possible excitations were allowed. The manganese 2p orbitals were placed in the RAS1 space, allowing a maximum of one excitation. Tests of RAS spectral sensitivity shows that good spectral quality can be achieved with relatively small basis sets and that many systems with weak ligands can be described without the use of large active spaces.[36,37] Core hole states were generated using a projection operator that selectively removes configurations with fully occupied core orbitals.[38,39] Core-excited states with $\Delta S = 0, \pm 1$ relative to the ground state were included in the calculations to satisfy the spin-selection rules of the electric dipole and the spin−orbit operator. Orbital optimization was performed using state-average RASSCF, performed separately for each spin multiplicity and irreducible representation. All possible states of each spin multiplicity were included in these calculations, using an efficient configuration interaction algorithm to converge the state-average calculations.[40] To avoid orbital rotation, i.e., that the hole appears in a higher-lying orbital, the core orbitals have been frozen in the final states. The Douglas−Kroll−Hess Hamiltonian is used to describe scalar relativistic effects.[41,42] RASPT2 calculations were performed with the default ionization potential electron affinity shift of 0.25 hartree (6.8 eV) and an imaginary shift of 0.3 hartree (8.2 eV). Results for calculations with different imaginary shift are shown in Supporting Information, Figure S3. Spin−orbit coupling is described by a RAS state-interaction (RASSI) approach.[43,44] The calculated spectra were convoluted with a Lorentzian of 0.34 eV full width at half-maximum (FWHM) for the L_3 edge, and 0.39 eV FWHM for the L_2 edge, to account for core hole lifetime broadening.[45] The experimental broadening is simulated with an additional Gaussian broadening of 0.2 eV (FWHM). Calculated spectra were shifted in energy to align with the experimental spectra, see the Supporting Information for details.

Crystal field (CF) and CTM simulations were performed using the CTM4XAS 5.5 software package.[46] Parameters employed for simulating $L_{2,3}$ edge spectra of $Mn(acac)^{+}_{n}$, n = 1−3, are given in Supporting Information, Table S1. Simulated spectra were shifted in energy to match the experimental spectra as given in Supporting Information, Table S3. Both Lorentzian (0.34 eV FWHM for L_3 and 0.39 eV FWHM for L_2) and Gaussian broadening (0.2 eV FWHM) was applied[45] while Slater integrals have been scaled to 80% of their atomic value. CF calculations were performed for a broad range of CF

https://doi.org/10.1021/acs.jpca.3c02794
J. Phys. Chem. A 2023, 127, 7121−7131

strength, varying parameters 10*Dq*, *Dt*, and *Ds* for their respective symmetries.[47]

RESULTS AND DISCUSSION

Ground-State Structures. The DFT-optimized ground-state structure of $Mn(acac)_1^+$ is shown in Figure 1. The molecule adopts a C_{2v} symmetry identical to the prediction of isoelectronic $Cr(acac)_1$.[48] There are, however, slight differences in transition-metal−oxygen bond lengths that become shortened in $Mn(acac)_1^+$ (1.900 Å) compared to $Cr(acac)_1$ (2.015 Å). Since the transition-metal monoacetylonates have not been stabilized in the condensed phase or as solvated species, there is no experimental data on the structure of $Mn(acac)_1^+$.

For $Mn(acac)_2^+$, a square planar and a slightly distorted square planar structure are almost degenerate with an energy separation of 0.2 kcal/mol, with the former slightly favored by DFT (B3LYP) and the latter slightly favored by CASPT2. Considering the small energy differences, these calculations do not provide a definitive assignment of the structure. In the following, we will discuss the square planar structure, also shown in Figure 1, that is in line with the ground-state structure of isoelectronic $Cr(acac)_2$[48,49] and proposed planar structure for other $3d^4$ metal−ligand complexes.[50] Changes in the electronic structure of both geometries are minor, and results for the distorted structure are shown in the Supporting Information. However, the structure is distinctively different from bulk, solvated, and neutral gas-phase $Mn(acac)_2$ that is a three-dimensional structure of tetrahedral symmetry.[50−53]

Finally, in the fully coordinated $Mn(acac)_3^+$ the Mn central atom is locally octahedrally coordinated, a ball-and-stick model is shown in Figure 1. While the neutral $Mn(acac)_3$ is Jahn-Teller distorted resulting in a tetragonally elongated octahedral form,[4,50,54] the cationic species shows an octahedrally coordinated Mn central atom, which is expected as there is no energy gain in Jahn-Teller distortion with the central Mn atom in oxidation state +4 as will be discussed in detail later.

Electronic Structure of $Mn(acac)_n^+$ Deduced from Mn $L_{2,3}$ Edge X-ray Absorption Spectroscopy. Experimental manganese $L_{2,3}$ edge spectra of $Mn(acac)_n^+$, n = 1−3 are presented in Figure 2 along with RASPT2 calculations[35] and CTM simulations.[46] Both ab initio and semi-empirical fitting models have been shown to give consistent descriptions of the coupling between spectra and electronic structure.[34,55] There is an overall satisfactory agreement between experimental spectra and RASPT2 calculations highlighting that the applied theory is capable of capturing the correlated nature of the electronic structure of $Mn(acac)_n^+$, n = 1−3.[48,56] Furthermore, from a comparison of the experimental spectra to the CF/CTM simulations empirical system parameters such as the CF strength parameter 10*Dq* can be extracted.

The spectrum of $Mn(acac)_1^+$ is dominated by an almost atomic-like multiplet structure of the manganese metal center adopting a local $3d^5$ electronic configuration.[57−59] There is, however, a slight splitting of the leading line at the L_3 edge (at about 639.5 eV) also indicated by the dashed lines in Figure 2 that can be traced back to the CF splitting in a C_{2v} symmetry caused by the acetylacetonate ligand pushing the $3d_{xy}$ orbital higher in energy as can be seen from a comparison to the CF simulation in Figure 2. In Supporting Information, Figure S4, we show a systematic study of the spectral changes as a function of CF strength and find that a CF strength 10*Dq* of −1.2 eV reproduces the spectrum of $Mn(acac)_1^+$ complex best.

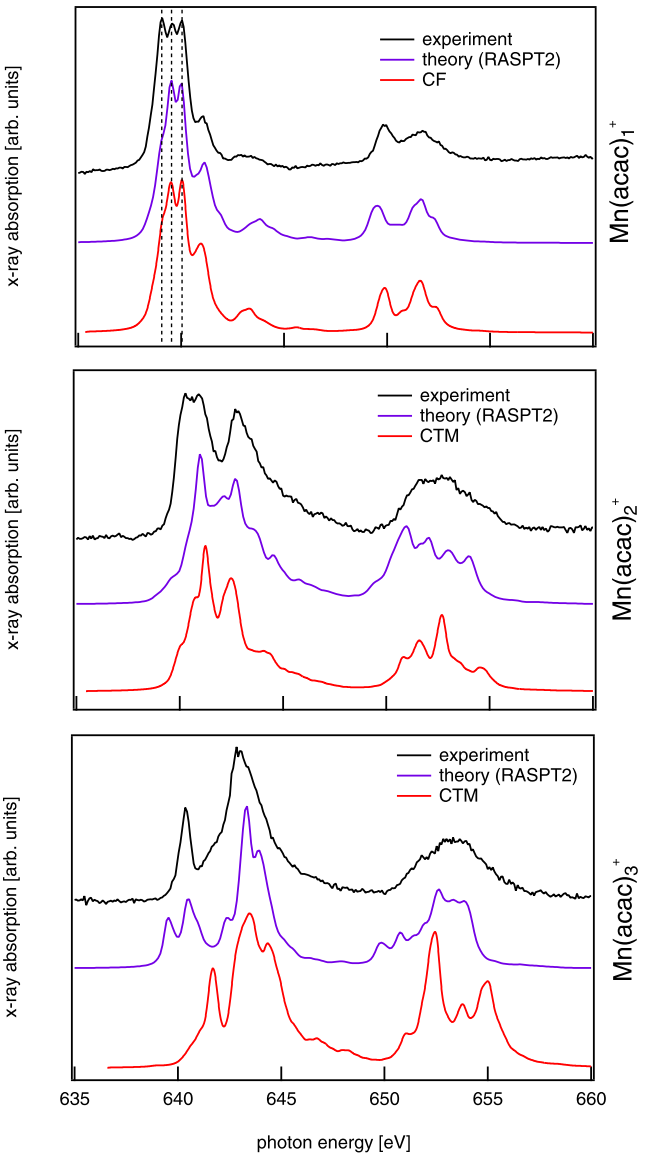

Figure 2. X-ray absorption spectra of gas-phase $Mn(acac)_n^+$, n = 1−3 at the Mn $L_{2,3}$ edges alongside RASPT2 calculations and CF/CTM simulations. From the RASPT2 calculations, $3d^5$, $3d^4$, and $3d^3$ local configurations of the Mn center were extracted for n = 1−3, respectively. Parameters of the CF/CTM calculations are given in Supporting Information, Table S1.

The complete set of parameters is given in Supporting Information, Table S1. Also, the RASPT2 calculation reproduces the experimental spectrum reasonably well and finds a mono-configurational, high-spin $^6A_1$ (C_{2v}, $a_1^1(3d_{x^2-y^2})a_1^1(3d_{z^2})a_2^1(3d_{xy})b_1^1(3d_{xz})b_2^1(3d_{yz})a_1^0(4s)$) ground state adopting the same multiplicity as the isoelectronic neutral $Cr(acac)_1$ complex but with a different distribution of the electrons among 3d and 4s derived states resulting in a $^6B_2$ (C_{2v}, $a_1^1(3d_{x^2-y^2})a_1^1(3d_{z^2})a_2^1(3d_{xy})b_1^1(3d_{xz})b_2^0(3d_{yz})a_1^1(4s)$) ground state for neutral $Cr(acac)_1$.[48] Note that the electronic configuration of $Mn(acac)_1^+$ does not change when adding the 4s orbital to the active space. The mono-configurational nature and the fact that the experimental spectrum can be reasonably well reproduced by a CF simulation only, implies that there is little ligand−metal or metal−ligand charge transfer and hybridization. Moreover, in $Mn(acac)_1^+$ we find a DFT and

https://doi.org/10.1021/acs.jpca.3c02794
J. Phys. Chem. A 2023, 127, 7121−7131

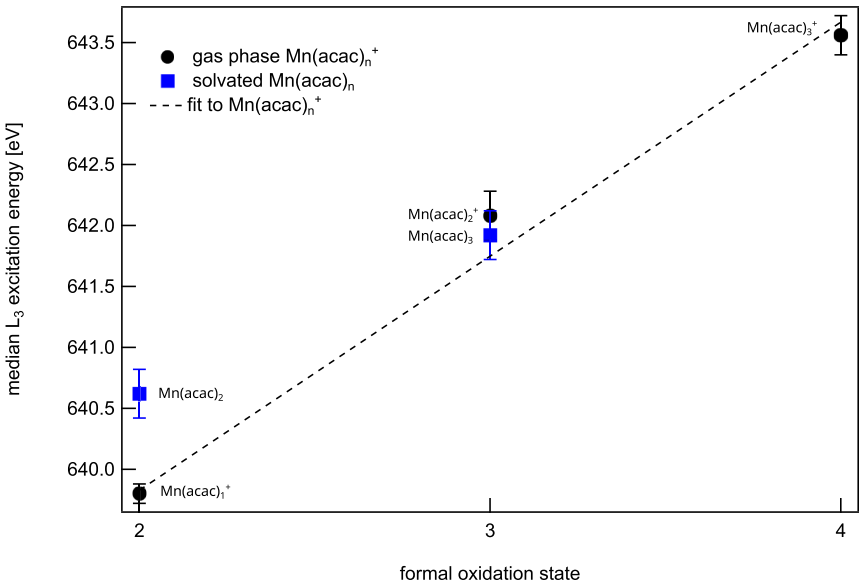

Figure 3. Experimentally determined median L_3 excitation energy as a function of formal oxidation state for gas-phase $Mn(acac)^+_{1-3}$ (this study) and solvated, neutral $Mn(acac)_{2,3}$ (extracted from ref 70). The linear fit to the gas-phase data gives a slope of 1.9 ± 0.1 eV per oxidation state and an offset of 636.2 ± 0.2 eV, respectively.

RAS Mulliken spin density at the Mn atom of 4.83 and 4.92, respectively. Since the Mulliken spin is known to correlate strongly with the Mn oxidation state,[60] our results indicate an oxidation state of +2, which is in line with the findings discussed above.

The spectrum of $Mn(acac)^+_2$ can neither be characterized as dominated by atomic multiplets nor by CF splitting making simulation of the spectrum using a CF approach rather challenging. We were, however, able to reasonably well reproduce the L_3 edge of $Mn(acac)^+_2$ by simulating the spectrum in a simplified square planar symmetry using a CF strength of 2.4 eV and employing charge transfer, which is consistent with the RAS result of orbital energetic ordering. Moreover, from the RASPT2 calculations we can determine the ground state to be a high-spin ^5A (C_2) state with four occupied, localized 3d orbitals, which corresponds to an oxidation state of +3 of the manganese metal center. This is further substantiated by a DFT and RAS Mulliken spin population at the Mn atom of 3.99 and 3.90, respectively. This is also in line with isoelectronic $Cr(acac)_2$ in $^5B_{1g}$ (D_{2h}) ground state, where four 3d electron state-derived orbitals are singly occupied.

Interestingly neutral $Mn^{III}(acac)_3$ and cationic $Mn^{III}(acac)^+_2$ can be both approximated as high-spin $3d^4$ systems in a (pseudo-)tetragonal square planar symmetry[4,50,54,61,62] and might result in similar spectral shapes at the manganese $L_{2,3}$ edges. Indeed, the magnitude of the splitting of the L_3 line of 1.7 eV is comparable in neutral $Mn(acac)_3$[63,64] and cationic $Mn(acac)^+_2$ (see Supporting Information, Figure S10). Still, there are distinct differences in the spectral shape, while the mean excitation energy is similar as discussed in the next section. Although the effect of changing the geometry within a defined oxidation state has been explored previously, highlighting a redistribution of spectral weight without inducing larger energetic shifts,[63,65] we speculate that the observed spectral differences between $Mn^{III}(acac)_3$ and $Mn^{III}(acac)^+_2$ are due to a re-ordering of the 3d orbitals induced by the additional ligand in z-direction in $Mn(acac)_3$. The additional ligand results in an energy penalty for the $3d_{z^2}$ orbital pushing it up in energy and switching the order with other occupied 3d orbitals. Again, both neutral $Mn^{III}(acac)_3$ and cationic $Mn^{III}(acac)^+_2$ exist in high-spin $3d^4$ configuration, but the different order of the same occupied orbitals changes the spectral shape.

Finally, a comparison of the experimental manganese $L_{2,3}$ edge spectrum and the RAS/CTM calculations of the fully coordinated $Mn(acac)^+_3$ complex is shown in Figure 2. The spectrum is dominated by CF splitting and the spectral features strongly resemble other Mn^{IV} species in bulk in O_h symmetry.[66] However, to achieve an even better agreement between the experimental and CF/CTM simulated spectrum it is necessary to involve finite hybridization via charge transfer similar to the case of isoelectronic $Cr(acac)_3$.[65] The CF strength parameter $10Dq$ of 2.1 eV extracted from the simulations indicates a high-spin state[59] and agrees well with values deduced from UV−vis experiments of 2.1 eV[67] and 2.4 eV[68] for neutral $Mn(acac)_3$. These findings are consistent with our RASSCF calculations that predict a high-spin ^4A (C_2) ground state in agreement with isoelectronic $Cr(acac)_3$.[48] Hence, $Mn(acac)^+_3$ is shown to be in oxidation state +4 further evidenced by DFT and RAS Mulliken spin populations of 3.03 and 2.69, respectively, at the Mn center.

As a summary, the CF/CTM simulations indicate that metal−ligand hybridization is negligible in $Mn(acac)^+_1$ while playing an increasing role in $Mn(acac)^+_{2,3}$ as expected from the increasing oxidation state of the metal.[69] We also identified the oxidation states of the manganese atoms for all the complexes by comparison to CF/CTM and RAS calculations as well as by analyzing Mulliken spin populations, also matching the formal oxidation states.

Comparison of L_3 Excitation Energy Shifts in Cationic and Neutral $Mn(acac)^{+,0}_n$. Analyzing L_3 excitation energy shifts is a well-established tool to infer oxidation states from $L_{2,3}$ edge XAS.[66,71,72] Experimentally determined median L_3 excitation energies of $Mn(acac)^+_n$, n = 1−3, are shown in Figure 3 as a function of formal oxidation states. As expected they scale linearly, further substantiating our oxidation state assignments from analyzing spectral shapes at the manganese

https://doi.org/10.1021/acs.jpca.3c02794
J. Phys. Chem. A 2023, 127, 7121−7131

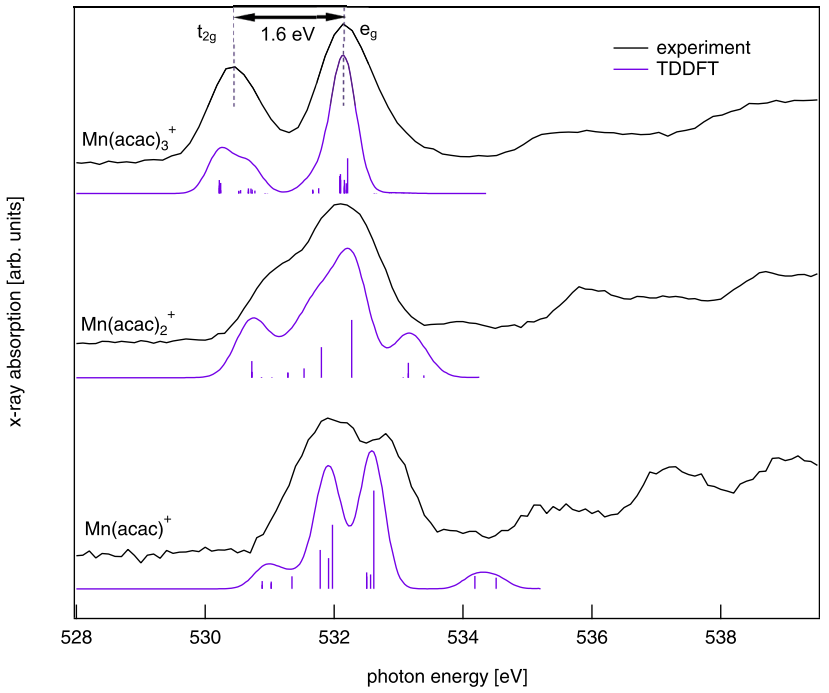

Figure 4. X-ray absorption spectra of gas-phase $Mn(acac)_n^+$, n = 1−3, at the oxygen K-edge alongside TD-DFT calculations.

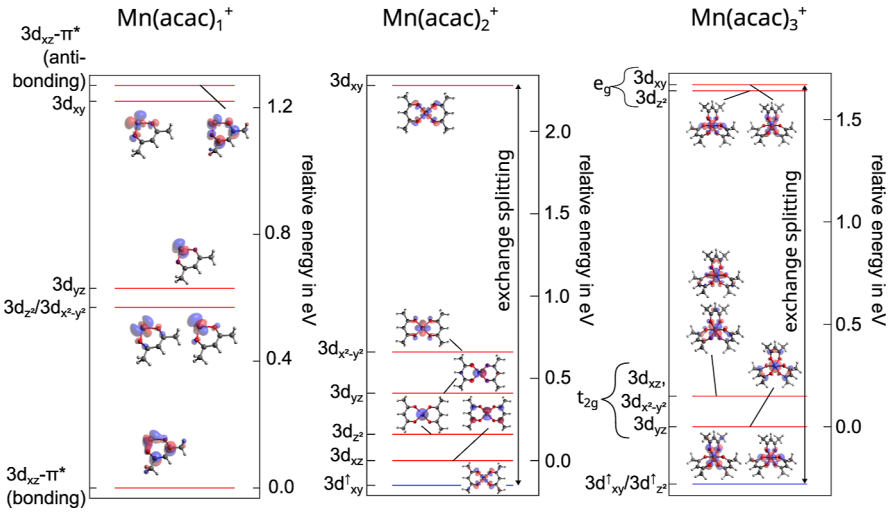

Figure 5. Energetic ordering of unoccupied molecular orbitals with significant Mn 3d or 4s character extracted from the oxygen K-edge of $Mn(acac)_n^+$, n = 1−3. Blue and red lines correspond to unoccupied spin up and down states, respectively. The origin of the relative energy scale is set to the lowest unoccupied minority spin state with significant 3d character. Isosurface plots with an isosurface value = 0.4 of these molecular orbitals are shown as well.

$L_{2,3}$ edge. The extracted slope of 1.9 ± 0.1 eV per oxidation state is well within the range of reported values for Mn ranging from 0.8−2 eV.[66,71−74] Interestingly, the shift for $Mn(acac)_n^+$ complexes, n = 1−3, is significantly larger than the reported shift of 0.95 ± 0.02 eV for cationic manganese oxide clusters,[74] which might be attributed to the different bond character in $Mn(acac)_{1-3}^+$ and MnO_{1-4}^+. Additionally, we show the median manganese L_3 excitation energy as a function of oxidation state for neutral $Mn(acac)_n^0$ complexes, n = 2, 3.

RASPT2 calculations of the oxidation shift of Mn complexes have previously shown deviations of no more than 0.3 eV per oxidation state.[63,74] Here, the presence of intruder states in some RASPT2 calculations, especially for $Mn(acac)_3^+$, results in a strong dependence of edge position on the choice of imaginary shift, see Supporting Information, Figure S3, which prevents an accurate prediction of the oxidation state shift. At the RASSCF level, the oxidation state shifts are predicted with a deviation of 0.5 eV per oxidation state.

There is a striking difference in the L_3 excitation energy of 0.8 eV for oxidation state +2 when comparing neutral $Mn^{II}(acac)_2$ and cationic $Mn^{II}(acac)_1^+$. The shift toward higher excitation energy could be induced by a reduced fractional 3d occupation in $Mn^{II}(acac)_2$ still representing the same oxidation state of +2.[75] However, in both cases the X-ray absorption spectrum at the Mn $L_{2,3}$ edges could reasonably well be reproduced by CF simulations only and DFT calculations give the same Mulliken spin population[63] indicating the same or at least very similar 3d occupation in both cases. It previously has

https://doi.org/10.1021/acs.jpca.3c02794
J. Phys. Chem. A 2023, 127, 7121−7131

been shown that the excitation energy systematically decreases within one oxidation state when decreasing the average coordination of the metal center.[76] A change in excitation energy of the order of 0.25 eV per change in coordination number has been reported.[76] Since the coordination number of neutral $Mn^{II}(acac)_2$ and cationic $Mn^{II}(acac)_1^+$ differs by two, we attribute the observed shift to the different coordination of the metal center in both species.

On the other hand, the same L_3 excitation energy is observed for cationic and neutral $Mn(acac)_n^{0,+}$ in oxidation state +3. As discussed in the previous section, despite the fact that the metal centers in $Mn^{III}(acac)_3$ and $Mn^{III}(acac)_2^+$ exist in nominal different symmetries, the strong Jahn−Teller distortion pushing two of the oxygen atoms away from the metal center resulting in an effective lowering of the coordination number to four, the same as in $Mn^{III}(acac)_2^+$ thereby resulting in very similar L_3 excitation energies.

We want to emphasize that the variation in L_3 excitation energy due to varying coordination, although sizable, is a second-order effect and the shift is still dominated by the oxidation state of the metal center in these high-spin states.

Oxygen K-Edge Spectroscopy and Energetic Ordering of the 3d Orbitals. In order to get a more complete picture of the electronic structure of $Mn(acac)_n^+$, $n = 1-3$, we complement the measurements at the manganese $L_{2,3}$ edges with oxygen and carbon K-edge spectroscopy. In Figure 4 X-ray absorption spectra of gas-phase $Mn(acac)_n^+$, $n = 1-3$, at the oxygen K-edge are shown. The experimental X-ray absorption spectra are compared to theoretical spectra from TD-DFT calculations. Low-energy transitions are reproduced well, while high-energy transitions are known to be less well reproduced due to approximations employed in TD-DFT.[77] Hence, we are focusing the analysis to the low-energy region between 530 and 534 eV.

The good agreement of calculated and experimental spectra allows us to identify the molecular orbitals involved in the individual transitions represented as sticks in Figure 4. However, we are focusing only on those molecular orbitals that are hybrids of ligand[78] and metal (manganese) 3d valence states.[48,79] From the relative excitation energies into these molecular orbitals, we deduce an energetic ordering of the unoccupied 3d derived states as shown in Figure 5 along with isosurface plots of the respective molecular orbitals. All other transitions shown in Figure 4 are dominated by transitions into ligand type orbitals and are therefore omitted in Figure 5.

In the $Mn(acac)_1^+$ complex, the orbitals with strong $3d_{yz}$, $3d_{z^2}$, and $3d_{x^2-y^2}$ character group together within 0.2 eV being basically degenerate, while the $3d_{xy}$ orbital is pushed up in energy by about 0.6 eV. This is expected from a simple CF picture[48] where the $3d_{xy}$ orbital has the highest density along the metal−oxygen bond. However, within the CF picture we would also expect the $3d_{xz}$ orbital to group with the $3d_{yz}$, $3d_{z^2}$, and $3d_{x^2-y^2}$ orbitals but instead the DFT calculation predicts a strong hybridization of the $3d_{xz}$ orbital with a ligand π^* orbital resulting in the formation of bonding and antibonding molecular orbitals well separated in energy shifting the transitions related to the bonding and antibonding orbitals symmetrically down and up by about 0.6 eV, respectively. These transitions also lead to the largest discrepancies between the calculated and experimental spectra with an otherwise good agreement. Furthermore, the hybridization of the $3d_{xz}$ orbital is in contrast to the analysis of the Mn $L_{2,3}$ edge spectra pointing to negligible hybridization of all the 3d states with the ligand orbitals. Hence, it seems that the strong hybridization of the $3d_{xz}$ orbital with ligand orbitals resulting in transitions at 531.4 and 532.6 eV are rather artifacts of the employed approximations to DFT that are known to over-delocalize 3d orbitals.[80]

In the $Mn(acac)_2^+$ complex, orbitals with $3d_{z^2}$, $3d_{yz}$, $3d_{x^2-y^2}$, and $3d_{xz}$ character are distributed over 0.7 eV instead of being tightly bunched together as in $Mn(acac)_1^+$. This is expected in a square planar symmetry as the degeneracy of the $3d_{yz}$, $3d_{xz}$, $3d_{x^2-y^2}$, and $3d_{z^2}$ orbitals is lifted by the lower symmetry of the system compared to the only weakly disturbed local spherical symmetry of Mn in $Mn(acac)_1^+$. Since, there is no ligand in z-direction, the $3d_{z^2}$ orbital should be lowest in energy experiencing the smallest influence of the ligand field of all the 3d orbitals. However, the orbital with $3d_{xz}$ character is slightly lower in energy by about 160 meV showcasing that the more subtle details of the electronic structure cannot be fully explained by CF theory alone but must also take into account the covalent bonding of the metal center to the ligands.

In the case of the $Mn(acac)_3^+$ complex, the orbitals group nicely into t_{2g} and e_g orbitals as expected[52,65,81] in a local octahedral symmetry of the metal center. The average energy separation between the t_{2g} and e_g orbitals is 1.6 eV also indicated in Figure 4. A similar analysis of the oxygen K-edge has been applied to isoelectronic $Cr(acac)_3$ in a condensed form, however, in contrast the t_{2g}- and e_g-like states could not be clearly disentangled and the splitting of the main resonance in the oxygen K-edge spectrum is only about 1 eV[81] while it is 1.6 eV in the case of cationic $Mn(acac)_3^+$.

The overall grouping of the 3d states for all $Mn(acac)_n^+$ complexes, $n = 1-3$, is dominated by the CF as present in the respective systems and has been proposed before.[48] Moreover, we are able to quantify the CF splitting as extracted from the experimental data by comparison to the TD-DFT calculations. Although different definitions could be applied and therefore result in slightly different absolute values, we follow the approach as outlined in ref 48, where the CF is defined as the energy separation of the $3d_{xz,yz}$ and $3d_{xy}$ orbitals. Since the $3d_{xz}$ and $3d_{yz}$ orbitals are not degenerate here, we opted for the average $3d_{xz,yz}-3d_{xy}$ energy separation to quantify the CF splitting. Furthermore, in the case of $Mn(acac)_{2,3}^+$ we can additionally extract the exchange splitting from the oxygen K-edge spectrum as the energetic separation of $3d_{xy}^{\uparrow}$ and $3d_{xy}^{\downarrow}$ and energetically almost degenerate $3d_{xy}^{\uparrow}$, $3d_{z2}^{\uparrow}$, $3d_{xy}^{\downarrow}$, and $3d_{z2}^{\downarrow}$ states, respectively. This results in an exchange splitting of 2.4 eV for $n = 2$ and 2.0 eV for $n = 3$ as shown in Figure 5. These values are in line with rough estimates of an average value of 0.6 eV per unpaired spin.[77,82] Again, the robustness of this approach is achieved by linking the experimental spectrum with the TD-DFT calculation to extract the energetic position of the unoccupied 3d orbitals. Extracting exchange and CF splittings from virtual orbitals alone could possibly not be very reliable as they strongly depend on the leftover basis functions and choice of the functional.

While showing a similar trend with increasing number of ligands, the values of the CF parameters extracted from the oxygen K-edge (0.6, 2.1, 1.6 eV) are systematically smaller than the $10Dq$ parameters extracted from the CF/CTM simulations (1.2, 2.4, 2.1 eV) of the manganese $L_{2,3}$ edges. Deducing CF splittings directly from metal L-edge spectra is often hindered by the presence of multiplet splittings. However, in rare cases

https://doi.org/10.1021/acs.jpca.3c02794
J. Phys. Chem. A 2023, 127, 7121−7131

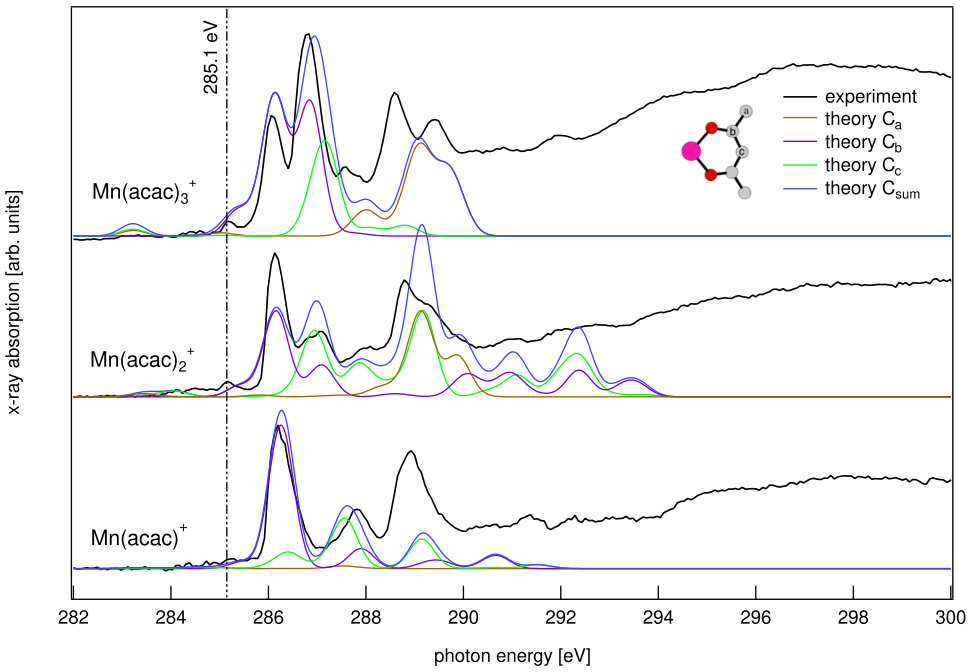

Figure 6. X-ray absorption spectra of gas-phase $Mn(acac)_n^+$, n = 1−3, at the carbon K-edge alongside TD-DFT calculations.

where the spectrum is dominated by CF splittings as for example in neutral $Cr(acac)_3$[81] they closely match the values extracted from oxygen K-edge spectra of isoelectronic $Mn(acac)_3^+$. Hence, showing that the 10Dq parameters, which are inputs to the CTM simulations, do not necessarily equal the apparent CF splittings as extracted from measured or simulated manganese $L_{2,3}$ edge spectra. However, both show the same dependence on the number of ligands.

The electronic structure in $Mn(acac)_n^+$, n = 1−3, is dominated by a competition between CF strength and exchange energy. As discussed above, we can extract an exchange splitting from a comparison of experimental and TD-DFT-calculated oxygen K-edge spectrum, which is 2.4 and 2 eV in $Mn(acac)_{2,3}^+$, respectively, and is expected to be even larger in $Mn(acac)_1^+$. The CF splitting in $Mn(acac)_1^+$ is significantly smaller than the exchange energy resulting in an almost atomic-like X-ray absorption signal at the manganese $L_{2,3}$ edges. In $Mn(acac)_{2,3}^+$, however, CF and exchange splitting are of the same magnitude, i.e., ∼2 eV. Hence, they have to be treated on the same footing making it more challenging to describe the electronic structure at the metal center correctly. Therefore, advanced multireference methods such as RASPT2 have to be employed to reproduce the spectral features satisfactorily.

Carbon K-Edge Spectroscopy. The last piece of information on the electronic structure results from the analysis of the carbon K-edge spectrum. In Figure 6, X-ray absorption spectra of gas-phase $Mn(acac)_n^+$, n = 1−3, at the carbon K-edge are shown and compared to theoretical spectra from TD-DFT calculations. We again focus our analysis at the low energies from 284 to 290 eV, where the spectrum can reliably be reproduced by the TD-DFT calculations.

Along the series there is a significant change of the leading low-energy line at about 286 eV, while higher-energy transitions are less affected. The low-energy transitions are dominated by transitions into orbitals with large contributions of the carbon atoms next to the metal−oxygen bridge (labeled C_b in the inset of Figure 6).

Similarly, in acetylacetone it has been shown that the leading line in the spectrum at about 286 eV is dominated by transitions into orbitals with C_b character and that the energetic position strongly depends on a chemical shift of the core 1s electrons induced by the proximity to the more electronegative oxygen atoms.[83]

The pre-peak at 285.1 eV highlighted by the dashed line in Figure 6 is the only transition at the carbon K-edge into orbitals with significant metal 3d character[69] as inferred from a comparison to the TD-DFT calculations. The amount of metal 3d character in the valence orbitals decreases along the $Mn(acac)_n^+$ series, n = 1−3, substantiating the finding of an increase of the covalency of the metal−oxygen bond[84] as discussed earlier.

CONCLUSIONS

We studied and identified the electronic structure and oxidation state of cationic gas-phase $Mn(acac)_n^+$ complexes for the complete ligand series of n = 1−3 by combining XAS at the manganese $L_{2,3}$, the oxygen as well as carbon K-edges with RAS/TD-DFT calculations and CF/CTM simulations. We find that in $Mn(acac)_1^+$ the electronic structure is dominated by exchange interaction with only a small influence of the ligands' CF, while in $Mn(acac)_{2,3}^+$ exchange and CF splitting are competing and have therefore to be treated on the same footing. Overall our findings are in agreement with predictions.[48] We have shown that empirical parameters such as CF strength and exchange splitting can not only be quantified by semi-empirical parametrized CF/CTM simulations or expensive wave function-based methods but also can be extracted from a comparison of experimental oxygen K-edge spectra and readily available TD-DFT calculations. This method can enable screening of metal complexes that might show exchange-enhanced reactivity[85] or undergo spin-state

https://doi.org/10.1021/acs.jpca.3c02794
J. Phys. Chem. A 2023, 127, 7121−7131

changes induced by geometrical changes of reaction intermediates.[86]

Furthermore, we extracted oxidation states from L_3 median excitation energy shifts for both cationic and neutral $Mn(acac)_n^{0,+}$. In the case of $Mn(acac)_n^{0,+}$ in the same oxidation state +2, we were able to disentangle the effects of varying 3d occupation[75] and coordination.[76] We show that this is a sizable effect of about 40−50% of the expected shift in L_3 excitation energy per oxidation state[66,71] and may be considered by spectroscopists employing L-edge shifts to determine oxidation states.

■ ASSOCIATED CONTENT

Supporting Information

The Supporting Information is available free of charge at https://pubs.acs.org/doi/10.1021/acs.jpca.3c02794.

Ground-state structures for all complexes, additional details on RASSCF and RASPT2 calculations, comparison of calculated oxygen K-edge spectra for planar and distorted structure of $Mn(acac)_2^+$, systematic CF and CTM modeling for all complexes, photofragmentation channels and partial ion yields at all edges investigated, and details on determining L_3 median excitation energy (PDF)

■ AUTHOR INFORMATION

Corresponding Author

Konstantin Hirsch − *Abteilung für Hochempfindliche Röntgenspektroskopie, Helmholtz-Zentrum Berlin für Materialien und Energie, 12489 Berlin, Germany;* orcid.org/0000-0001-5050-3026; Email: Konstantin.Hirsch@helmholtz-berlin.de

Authors

Olesya S. Ablyasova − *Physikalisches Institut, Albert-Ludwigs-Universität Freiburg, 79104 Freiburg, Germany; Abteilung für Hochempfindliche Röntgenspektroskopie, Helmholtz-Zentrum Berlin für Materialien und Energie, 12489 Berlin, Germany*

Meiyuan Guo − *SSRL, SLAC National Accelerator Laboratory, Menlo Park, California 94025, United States; Department of Chemistry-Ångström Laboratory, Uppsala University, SE-75120 Uppsala, Sweden;* orcid.org/0000-0003-2474-6264

Vicente Zamudio-Bayer − *Abteilung für Hochempfindliche Röntgenspektroskopie, Helmholtz-Zentrum Berlin für Materialien und Energie, 12489 Berlin, Germany;* orcid.org/0000-0002-4038-0584

Markus Kubin − *Abteilung für Hochempfindliche Röntgenspektroskopie, Helmholtz-Zentrum Berlin für Materialien und Energie, 12489 Berlin, Germany;* orcid.org/0000-0002-2209-9385

Tim Gitzinger − *Physikalisches Institut, Albert-Ludwigs-Universität Freiburg, 79104 Freiburg, Germany; Abteilung für Hochempfindliche Röntgenspektroskopie, Helmholtz-Zentrum Berlin für Materialien und Energie, 12489 Berlin, Germany*

Mayara da Silva Santos − *Physikalisches Institut, Albert-Ludwigs-Universität Freiburg, 79104 Freiburg, Germany; Abteilung für Hochempfindliche Röntgenspektroskopie, Helmholtz-Zentrum Berlin für Materialien und Energie, 12489 Berlin, Germany*

Max Flach − *Physikalisches Institut, Albert-Ludwigs-Universität Freiburg, 79104 Freiburg, Germany; Abteilung für Hochempfindliche Röntgenspektroskopie, Helmholtz-Zentrum Berlin für Materialien und Energie, 12489 Berlin, Germany*

Martin Timm − *Abteilung für Hochempfindliche Röntgenspektroskopie, Helmholtz-Zentrum Berlin für Materialien und Energie, 12489 Berlin, Germany*

Marcus Lundberg − *Department of Chemistry-Ångström Laboratory, Uppsala University, SE-75120 Uppsala, Sweden;* orcid.org/0000-0002-1312-1202

J. Tobias Lau − *Physikalisches Institut, Albert-Ludwigs-Universität Freiburg, 79104 Freiburg, Germany; Abteilung für Hochempfindliche Röntgenspektroskopie, Helmholtz-Zentrum Berlin für Materialien und Energie, 12489 Berlin, Germany;* orcid.org/0000-0003-0976-6902

Complete contact information is available at: https://pubs.acs.org/10.1021/acs.jpca.3c02794

Author Contributions

M.K., V.Z.B., and J.T.L.: conceived the experiment. M.K., V.Z.B., M.T., T.G., and J.T.L.: planned the experiment. M.K., V.Z.B., M.T., M.F., M.S.S, O.S.A., and T.G.: carried out the experiment. O.S.A., V.Z.B., K.H., M.K., and J.T.L.: analyzed the experimental data. M.G. and M.L.: carried out the DFT and RAS calculations. O.S.A., V.Z.B., and K.H.: carried out CF/CTM calculations. M.G., M.L., O.S.A., V.Z.B., and K.H.: analyzed the calculations. All authors discussed the results. O.S.A., V.Z.B., and K.H.: wrote the manuscript.

Notes

The authors declare no competing financial interest.

■ ACKNOWLEDGMENTS

Beamtime for this project was granted at the Ion Trap endstation of BESSY II, beamline UE52-PGM, operated by Helmholtz-Zentrum Berlin. This project has received funding from the German Federal Ministry of Education and Research through grant no. BMBF-05K16VF1. J.T.L., M.F., M.S.S., and O.S.A. acknowledge support by the DFG funded Research Training Group "Dynamics of Controlled Atomic and Molecular Systems" (RTG 2717). M.G. acknowledges a Knut and Alice Wallenberg Foundation postdoctoral scholarship (KAW2019.0559). M.L. acknowledges financial support from the Swedish Research Council (VR 2022-04794). Computations were partly performed on resources provided by the Swedish National Infrastructure for Computing (SNIC) under project SNIC2022-22-837, partially funded by the Swedish Research Council through grant agreement no. 2018-05973.

■ REFERENCES

(1) Sleightholme, A. E. S.; Shinkle, A. A.; Liu, Q.; Li, Y.; Monroe, C. W.; Thompson, L. T. Non-Aqueous Manganese Acetylacetonate Electrolyte for Redox Flow Batteries. *J. Power Sources* **2011**, *196*, 5742−5745.

(2) Suttil, J. A.; Kucharyson, J. F.; Escalante-Garcia, I. L.; Cabrera, P. J.; James, B. R.; Savinell, R. F.; Sanford, M. S.; Thompson, L. T. Metal Acetylacetonate Complexes for High Energy Density Non-Aqueous Redox Flow Batteries. *J. Mater. Chem. A* **2015**, *3*, 7929−7938.

(3) Avci-Camur, C.; Perez-Carvajal, J.; Imaz, I.; Maspoch, D. Metal Acetylacetonates as a Source of Metals for Aqueous Synthesis of Metal−Organic Frameworks. *ACS Sustainable Chem. Eng.* **2018**, *6*, 14554−14560.

(4) Liedy, F.; Eng, J.; McNab, R.; Inglis, R.; Penfold, T. J.; Brechin, E. K.; Johansson, J. O. Vibrational Coherences in Manganese Single-Molecule Magnets after Ultrafast Photoexcitation. *Nat. Chem.* **2020**, *12*, 452−458.
(5) Morgan, G. G.; Murnaghan, K. D.; Müller-Bunz, H.; McKee, V.; Harding, C. J. A Manganese(III) Complex That Exhibits Spin Crossover Triggered by Geometric Tuning. *Angew. Chem.* **2006**, *118*, 7350−7353.
(6) Sodhi, R. K.; Paul, S. An Overview of Metal Acetylacetonates: Developing Areas/Routes to New Materials and Applications in Organic Syntheses. *Catal. Surv. Asia* **2018**, *22*, 31−62.
(7) Broere, D. L. J.; Plessius, R.; van der Vlugt, J. I. New avenues for ligand-mediated processes − expanding metal reactivity by the use of redox-active catechol, o-aminophenol and o-phenylenediamine ligands. *Chem. Soc. Rev.* **2015**, *44*, 6886−6915.
(8) Vinum, M. G.; Voigt, L.; Hansen, S. H.; Bell, C.; Clark, K. M.; Larsen, R. W.; Pedersen, K. S. Ligand field-actuated redox-activity of acetylacetonate. *Chem. Sci.* **2020**, *11*, 8267−8272.
(9) Barber, J. Photosynthetic water splitting by the $Mn_4Ca^{2+}O_X$ catalyst of photosystem II: its structure, robustness and mechanism. *Q. Rev. Biophys.* **2017**, *50*, No. e13.
(10) Lubitz, W.; Chrysina, M.; Cox, N. Water oxidation in photosystem II. *Photosynth. Res.* **2019**, *142*, 105−125.
(11) Cox, N.; Pantazis, D. A.; Lubitz, W. Current Understanding of the Mechanism of Water Oxidation in Photosystem II and Its Relation to XFEL Data. *Annu. Rev. Biochem.* **2020**, *89*, 795−820.
(12) Armstrong, F. A. Why Did Nature Choose Manganese to Make Oxygen? *Philos. Trans. R. Soc., B* **2007**, *363*, 1263−1270.
(13) Yano, J.; Yachandra, V. Mn4Ca Cluster in Photosynthesis: Where and How Water is Oxidized to Dioxygen. *Chem. Rev.* **2014**, *114*, 4175−4205.
(14) Werlé, C.; Schlichter, P. The Rise of Manganese-Catalyzed Reduction Reactions. *Synthesis* **2021**, *54*, 517−534.
(15) Son, J. Sustainable manganese catalysis for late-stage C−H functionalization of bioactive structural motifs. *Beilstein J. Org. Chem.* **2021**, *17*, 1733−1751.
(16) Crandell, D. W.; Xu, S.; Smith, J. M.; Baik, M.-H. Intramolecular Oxyl Radical Coupling Promotes O−O Bond Formation in a Homogeneous Mononuclear Mn-based Water Oxidation Catalyst: A Computational Mechanistic Investigation. *Inorg. Chem.* **2017**, *56*, 4435−4445.
(17) Charles, R. G.; Bryant, B. E. *Inorganic Syntheses*; John Wiley Sons, Ltd., 1963; pp 183−184.
(18) Arslan, E.; Lalancette, R. A.; Bernal, I. An historic and scientific study of the properties of metal(III) tris-acetylacetonates. *Struct. Chem.* **2017**, *28*, 201−212.
(19) Kryukov, A. I.; Tkachenko, Z. A.; Bukhtiyarov, V. K.; Kriss, E. E. The phototransfer of an electron in manganese (III) tris-acetylacetonate and bis-acetylacetonatotrifluoroacetate. *Theor. Exp. Chem.* **1983**, *19*, 176−182.
(20) Mangione, G.; Sambi, M.; Carlotto, S.; Vittadini, A.; Ligorio, G.; Timpel, M.; Pasquali, L.; Giglia, A.; Nardi, M. V.; Casarin, M. Electronic Structure of CuTPP and CuTPP(F) Complexes: A Combined Experimental and Theoretical Study II. *Phys. Chem. Chem. Phys.* **2016**, *18*, 24890−24904.
(21) Eckert, S.; Mascarenhas, E. J.; Mitzner, R.; Jay, R. M.; Pietzsch, A.; Fondell, M.; Vaz da Cruz, V.; Föhlisch, A. From the Free Ligand to the Transition Metal Complex: FeEDTA− Formation Seen at Ligand K-Edges. *Inorg. Chem.* **2022**, *61*, 10321−10328.
(22) Hirsch, K.; Lau, J. T.; Klar, P.; Langenberg, A.; Probst, J.; Rittmann, J.; Vogel, M.; Zamudio-Bayer, V.; Möller, T.; von Issendorff, B. X-Ray Spectroscopy on Size-Selected Clusters in an Ion Trap: From the Molecular Limit to Bulk Properties. *J. Phys. B: At., Mol. Opt. Phys.* **2009**, *42*, 154029.
(23) Bari, S.; Egorov, D.; Jansen, T.; Boll, R.; Hoekstra, R.; Techert, S.; Zamudio-Bayer, V.; Bülow, C.; Lindblad, R.; Leistner, G.; et al. Soft X-ray Spectroscopy as a Probe for Gas-Phase Protein Structure: Electron Impact Ionization from Within. *Chem.—Eur. J.* **2018**, *24*, 7631−7636.
(24) Weiss, M.; Follath, R.; Sawhney, K.; Zeschke, T. Absolute energy calibration for plane grating monochromators. *Nucl. Instrum. Methods Phys. Res., Sect. A* **2001**, *467−468*, 482−484. 7th Int. Conf. on Synchrotron Radiation Instrumentation
(25) Frisch, M.; Trucks, G.; Schlegel, H.; Scuseria, G.; Robb, M.; Cheeseman, J.; Scalmani, G.; Barone, V.; Mennucci, B.; Petersson, G.; et al. *Gaussian 09*, Revision A.1; Gaussian Inc., 2009.
(26) Becke, A. D. Density-functional thermochemistry. III. The role of exact exchange. *J. Chem. Phys.* **1993**, *98*, 5648−5652.
(27) Stephens, P. J.; Devlin, F. J.; Chabalowski, C. F.; Frisch, M. J. Ab Initio Calculation of Vibrational Absorption and Circular Dichroism Spectra Using Density Functional Force Fields. *J. Phys. Chem.* **1994**, *98*, 11623−11627.
(28) Rassolov, V. A.; Pople, J. A.; Ratner, M. A.; Windus, T. L. 6-31G* basis set for atoms K through Zn. *J. Chem. Phys.* **1998**, *109*, 1223−1229.
(29) Finley, J.; Malmqvist, P. Å.; Roos, B. O.; Serrano-Andrés, L. The multi-state CASPT2 method. *Chem. Phys. Lett.* **1998**, *288*, 299−306.
(30) Larsson, E. D.; Zobel, J. P.; Veryazov, V. Benchmarking ANO-R basis set for multiconfigurational calculations. *Electron. Struct.* **2022**, *4*, 014009.
(31) Fdez. Galván, I.; Vacher, M.; Alavi, A.; Angeli, C.; Aquilante, F.; Autschbach, J.; Bao, J. J.; Bokarev, S. I.; Bogdanov, N. A.; Carlson, R. K.; et al. OpenMolcas: From Source Code to Insight. *J. Chem. Theory Comput.* **2019**, *15*, 5925−5964.
(32) Josefsson, I.; Kunnus, K.; Schreck, S.; Föhlisch, A.; de Groot, F.; Wernet, P.; Odelius, M. Ab Initio Calculations of X-ray Spectra: Atomic Multiplet and Molecular Orbital Effects in a Multiconfigurational SCF Approach to the L-Edge Spectra of Transition Metal Complexes. *J. Phys. Chem. Lett.* **2012**, *3*, 3565−3570.
(33) Bokarev, S. I.; Dantz, M.; Suljoti, E.; Kühn, O.; Aziz, E. F. State-Dependent Electron Delocalization Dynamics at the Solute-Solvent Interface: Soft-X-Ray Absorption Spectroscopy and Ab Initio Calculations. *Phys. Rev. Lett.* **2013**, *111*, 083002.
(34) Pinjari, R. V.; Delcey, M. G.; Guo, M.; Odelius, M.; Lundberg, M. Restricted Active Space Calculations of L-edge X-ray Absorption Spectra: From Molecular Orbitals to Multiplet States. *J. Chem. Phys.* **2014**, *141*, 124116.
(35) Celani, P.; Werner, H.-J. Multireference Perturbation Theory for Large Restricted and Selected Active Space Reference Wave Functions. *J. Chem. Phys.* **2000**, *112*, 5546−5557.
(36) Pinjari, R. V.; Delcey, M. G.; Guo, M.; Odelius, M.; Lundberg, M. Cost and sensitivity of restricted active-space calculations of metal L-edge X-ray absorption spectra. *J. Comput. Chem.* **2016**, *37*, 477−486.
(37) Lundberg, M.; Delcey, M. G. *Transition Metals in Coordination Environments: Computational Chemistry and Catalysis Viewpoints*; Broclawik, E., Borowski, T., Radoń, M., Eds.; Springer International Publishing: Cham, 2019; pp 185−217.
(38) Guo, M.; Sørensen, L. K.; Delcey, M. G.; Pinjari, R. V.; Lundberg, M. Simulations of iron K pre-edge X-ray absorption spectra using the restricted active space method. *Phys. Chem. Chem. Phys.* **2016**, *18*, 3250−3259.
(39) Delcey, M. G.; Sørensen, L. K.; Vacher, M.; Couto, R. C.; Lundberg, M. Efficient calculations of a large number of highly excited states for multiconfigurational wavefunctions. *J. Comput. Chem.* **2019**, *40*, 1789−1799.
(40) Delcey, M. G.; Couto, R. C.; Sørensen, L. K.; FdezGalván, I.; Guo, M.; Lindh, R.; Lundberg, M. Exact semi-classical light−matter interaction operator applied to two-photon processes with strong relativistic effects. *J. Chem. Phys.* **2020**, *153*, 024114.
(41) Douglas, M.; Kroll, N. M. Quantum electrodynamical corrections to the fine structure of helium. *Ann. Phys.* **1974**, *82*, 89−155.
(42) Hess, B. A. Relativistic electronic-structure calculations employing a two-component no-pair formalism with external-field projection operators. *Phys. Rev. A: At., Mol., Opt. Phys.* **1986**, *33*, 3742−3748.

https://doi.org/10.1021/acs.jpca.3c02794
J. Phys. Chem. A 2023, 127, 7121−7131

(43) Malmqvist, P. Å.; Roos, B. O. The CASSCF state interaction method. *Chem. Phys. Lett.* **1989**, *155*, 189−194.
(44) Malmqvist, P. Å.; Roos, B. O.; Schimmelpfennig, B. The restricted active space (RAS) state interaction approach with spin−orbit coupling. *Chem. Phys. Lett.* **2002**, *357*, 230−240.
(45) Chen, M. H.; Crasemann, B.; Mark, H. Widths and Fluorescence Yields of Atomic L-Shell Vacancy States. *Phys. Rev. A: At., Mol., Opt. Phys.* **1981**, *24*, 177−182.
(46) Stavitski, E.; de Groot, F. M. F. The CTM4XAS Program for EELS and XAS Spectral Shape Analysis of Transition Metal L Edges. *Micron* **2010**, *41*, 687−694.
(47) de Groot, F.; Kotani, A. *Core Level Spectroscopy of Solids*; CRC Press: Boca Raton, 2008; p 116.
(48) Fernandes, G. F. S.; Pontes, M. A. P.; Machado, F. B. C.; Ferrão, L. F. A. Electronic Structure and Stability of Transition Metal Acetylacetonates TM(AcAc)n (TM = Cr, Fe, Co, Ni, Cu; n = 1, 2, 3). *Comput. Theor. Chem.* **2022**, *1207*, 113502.
(49) Cotton, F. A.; Rice, C. E.; Rice, G. W. The Crystal and Molecular Structures of Bis(2,4-Pentanedionato)Chromium. *Inorg. Chim. Acta* **1977**, *24*, 231−234.
(50) Berger, R. J. F.; Girichev, G. V.; Giricheva, N. I.; Petrova, A. A.; Tverdova, N. V. The Structure of Mn(Acac)3—Experimental Evidence of a Static Jahn−Teller Effect in the Gas Phase. *Angew. Chem., Int. Ed.* **2017**, *56*, 15751−15754.
(51) Grush, M. M.; Muramatsu, Y.; Underwood, J. H.; Gullikson, E. M.; Ederer, D. L.; Perera, R. C. C.; Callcott, T. A. Soft X-ray Emission and Absorption—a Comparative Study on the Sensitivity to Oxidation State and Ligand Environment of Transition Metal complexes. *J. Electron Spectrosc. Relat. Phenom.* **1998**, *92*, 225−229.
(52) Carlotto, S.; Sambi, M.; Vittadini, A.; Casarin, M. Mn(Acac)2 and Mn(Acac)3 Complexes, a Theoretical Modeling of Their L2,3-Edges X-ray Absorption Spectra. *Polyhedron* **2017**, *135*, 216−223.
(53) Berger, R. J. F.; Girichev, G. V.; Giricheva, N. I.; Otlyotov, A. A.; Petrova, A. A. Ligand Coordination in Bis(β-diketonato) d Metals: The Mn(II) Case of D_{2h} versus D_{2d} Symmetry. *Inorg. Chem.* **2019**, *58*, 4344−4349.
(54) Stults, B. R.; Marianelli, R. S.; Day, V. W. Distortions of the Coordination Polyhedron in High-Spin Manganese(III) Complexes. 3. Crystal and Molecular Structure of .Gamma.-Tris-(Acetylacetonato)Manganese(III): A Tetragonally Elongated Octahedral Form. *Inorg. Chem.* **1979**, *18*, 1853−1858.
(55) Pinjari, R. V.; Delcey, M. G.; Guo, M.; Odelius, M.; Lundberg, M. Erratum: "Restricted Active Space Calculations of L-edge X-ray Absorption Spectra: From Molecular Orbitals to Multiplet States" [J. Chem. Phys. 141, 124116 (2014)]. *J. Chem. Phys.* **2015**, *142*, 069901.
(56) Carlotto, S.; Sambi, M.; Vittadini, A.; Casarin, M. Theoretical Modeling of the L2,3-Edge X-ray Absorption Spectra of Mn(Acac)2 and Co(Acac)2 Complexes. *Phys. Chem. Chem. Phys.* **2016**, *18*, 2242−2249.
(57) Hirsch, K.; Zamudio-Bayer, V.; Ameseder, F.; Langenberg, A.; Rittmann, J.; Vogel, M.; Möller, T.; v Issendorff, B.; Lau, J. T.; Lau, J. T. 2p X-ray Absorption of Free Transition-Metal Cations Across the 3d Transition Elements: Calcium Through Copper. *Phys. Rev. A: At., Mol., Opt. Phys.* **2012**, *85*, 062501.
(58) Martins, M.; Godehusen, K.; Richter, T.; Wernet, P.; Zimmermann, P. Open Shells and Multi-Electron Interactions: Core Level Photoionization of the 3d Metal Atoms. *J. Phys. B: At. Mol. Opt. Phys.* **2006**, *39*, R79−R125.
(59) Laan, G. v. d.; Kirkman, I. W. The 2p Absorption Spectra of 3d Transition Metal Compounds in Tetrahedral and Octahedral Symmetry. *J. Phys.: Condens. Matter* **1992**, *4*, 4189−4204.
(60) Blomberg, M. R. A.; Siegbahn, P. E. M. A Comparative Study of High-Spin Manganese and Iron Complexes. *Theor. Chem. Acc.* **1997**, *97*, 72−80.
(61) Diaz-Acosta, I.; Baker, J.; Hinton, J. F.; Pulay, P. Calculated and Experimental Geometries and Infrared Spectra of Metal Tris-Acetylacetonates: Vibrational Spectroscopy as a Probe of Molecular Structure for Ionic Complexes. Part II. *Spectrochim. Acta, Part A* **2003**, *59*, 363−377.
(62) Forman, A.; Orgel, L. The Jahn-Teller Effect in Manganic Acetylacetonate. *Mol. Phys.* **1959**, *2*, 362−366.
(63) Kubin, M.; Guo, M.; Kroll, T.; Löchel, H.; Källman, E.; Baker, M. L.; Mitzner, R.; Gul, S.; Kern, J.; Föhlisch, A.; et al. Probing the Oxidation State of Transition Metal Complexes: A Case Study on How Charge and Spin Densities Determine Mn L-edge X-ray Absorption Energies. *Chem. Sci.* **2018**, *9*, 6813−6829.
(64) Kubin, M.; Kern, J.; Guo, M.; Källman, E.; Mitzner, R.; Yachandra, V. K.; Lundberg, M.; Yano, J.; Wernet, P. X-Ray-Induced Sample Damage at the Mn L-edge: A Case Study for Soft X-ray Spectroscopy of Transition Metal Complexes in Solution. *Phys. Chem. Chem. Phys.* **2018**, *20*, 16817−16827.
(65) Kubin, M.; Guo, M.; Ekimova, M.; Källman, E.; Kern, J.; Yachandra, V. K.; Yano, J.; Nibbering, E. T. J.; Lundberg, M.; Wernet, P. Cr L-Edge X-ray Absorption Spectroscopy of CrIII(Acac)3 in Solution with Measured and Calculated Absolute Absorption Cross Sections. *J. Phys. Chem. B* **2018**, *122*, 7375−7384.
(66) Cramer, S. P.; DeGroot, F. M. F.; Ma, Y.; Chen, C. T.; Sette, F.; Kipke, C. A.; Eichhorn, D. M.; Chan, M. K.; Armstrong, W. H.; Libby, E.; et al. Ligand Field Strengths and Oxidation States from Manganese L-edge Spectroscopy. *J. Am. Chem. Soc.* **1991**, *113*, 7937−7940.
(67) Piper, T. S.; Carlin, R. L. Crystal Spectra of Some Trisacetylacetonates. *Inorg. Chem.* **1963**, *2*, 260−263.
(68) Yamaguchi, K.; Sawyer, D. T. Redox Chemistry for the Mononuclear Tris(Picolinato)- Tris(Acetylacetonata)-and Tris(8-Quinolinata)Manganese(III) Complexes: Reaction Mimics for the Water-Oxidation Cofactor in Photosystem II. *Inorg. Chem.* **1985**, *24*, 971−976.
(69) Suntivich, J.; Hong, W. T.; Lee, Y.-L.; Rondinelli, J. M.; Yang, W.; Goodenough, J. B.; Dabrowski, B.; Freeland, J. W.; Shao-Horn, Y. Estimating Hybridization of Transition Metal and Oxygen States in Perovskites from O K-edge X-ray Absorption Spectroscopy. *J. Phys. Chem. C* **2014**, *118*, 1856−1863.
(70) Kubin, M.; Guo, M.; Ekimova, M.; Baker, M. L.; Kroll, T.; Källman, E.; Kern, J.; Yachandra, V. K.; Yano, J.; Nibbering, E. T. J.; et al. Direct Determination of Absolute Absorption Cross Sections at the L-Edge of Dilute Mn Complexes in Solution Using a Transmission Flatjet. *Inorg. Chem.* **2018**, *57*, 5449−5462.
(71) Schmid, H. K.; Mader, W. Oxidation States of Mn and Fe in Various Compound Oxide Systems. *Micron* **2006**, *37*, 426−432.
(72) Tan, H.; Verbeeck, J.; Abakumov, A.; Van Tendeloo, G. Oxidation State and Chemical Shift Investigation in Transition Metal Oxides by EELS. *Ultramicroscopy* **2012**, *116*, 24−33.
(73) Risch, M.; Stoerzinger, K. A.; Han, B.; Regier, T. Z.; Peak, D.; Sayed, S. Y.; Wei, C.; Xu, Z.; Shao-Horn, Y. Redox Processes of Manganese Oxide in Catalyzing Oxygen Evolution and Reduction: An in Situ Soft X-ray Absorption Spectroscopy Study. *J. Phys. Chem. C* **2017**, *121*, 17682−17692.
(74) Delcey, M. G.; Lindblad, R.; Timm, M.; Bülow, C.; Zamudio-Bayer, V.; von Issendorff, B.; Lau, J. T.; Lundberg, M. Soft X-ray Signatures of Cationic Manganese−Oxo Systems, Including a High-Spin Manganese(V) Complex. *Phys. Chem. Chem. Phys.* **2022**, *24*, 3598−3610.
(75) Flach, M.; Hirsch, K.; Timm, M.; Ablyasova, O. S.; da Silva Santos, M.; Kubin, M.; Bülow, C.; Gitzinger, T.; von Issendorff, B.; Lau, J. T.; et al. Iron L3-edge Energy Shifts for the Full Range of Possible 3d Occupations within the Same Oxidation State of Iron Halides. *Phys. Chem. Chem. Phys.* **2022**, *24*, 19890−19894.
(76) Bourdelle, F.; Lloret, E.; Durand, C.; Airaghi, L. Evaluation of Scanning Transmission X-ray Microscopy at the Mn L2,3-Edges as a Potential Probe for Manganese Redox State in Natural Silicates. *Phys. Chem. Miner.* **2021**, *48*, 18.
(77) Frati, F.; Hunault, M. O. J. Y.; de Groot, F. M. F. Oxygen K-edge X-ray Absorption Spectra. *Chem. Rev.* **2020**, *120*, 4056−4110.
(78) Lessard, R.; Cuny, J.; Cooper, G.; Hitchcock, A. P. Inner-shell excitation of gas phase carbonates and α,γ-dicarbonyl compounds. *Chem. Phys.* **2007**, *331*, 289−303.
(79) Lewis, F. D.; Salvi, G. D.; Kanis, D. R.; Ratner, M. A. Electronic Structure and Spectroscopy of Nickel(II), Palladium(II), and

https://doi.org/10.1021/acs.jpca.3c02794
J. Phys. Chem. A 2023, 127, 7121−7131

Platinum(II) Acetylacetonate Complexes. *Inorg. Chem.* **1993**, *32*, 1251−1258.
(80) Hasnip, P. J.; Refson, K.; Probert, M. I. J.; Yates, J. R.; Clark, S. J.; Pickard, C. J. Density Functional Theory in the Solid State. *Philos. Trans. R. Soc., A* **2014**, *372*, 20130270.
(81) Carlotto, S.; Floreano, L.; Cossaro, A.; Dominguez, M.; Rancan, M.; Sambi, M.; Casarin, M. The Electronic Properties of Three Popular High Spin Complexes [TM(Acac)3, TM = Cr, Mn, and Fe] Revisited: An Experimental and Theoretical Study. *Phys. Chem. Chem. Phys.* **2017**, *19*, 24840−24854.
(82) Laan, G. v. d.; Kirkman, I. W. The 2p Absorption Spectra of 3d Transition Metal Compounds in Tetrahedral and Octahedral Symmetry. *J. Phys.: Condens. Matter* **1992**, *4*, 4189−4204.
(83) Bhattacherjee, A.; Pemmaraju, C. D.; Schnorr, K.; Attar, A. R.; Leone, S. R. Ultrafast Intersystem Crossing in Acetylacetone via Femtosecond X-ray Transient Absorption at the Carbon K-Edge. *J. Am. Chem. Soc.* **2017**, *139*, 16576−16583.
(84) Wasinger, E. C.; de Groot, F. M. F.; Hedman, B.; Hodgson, K. O.; Solomon, E. I. L-Edge X-ray Absorption Spectroscopy of Non-Heme Iron Sites: Experimental Determination of Differential Orbital Covalency. *J. Am. Chem. Soc.* **2003**, *125*, 12894−12906.
(85) Shaik, S.; Chen, H.; Janardanan, D. Exchange-Enhanced Reactivity in Bond Activation by Metal−Oxo Enzymes and Synthetic Reagents. *Nat. Chem.* **2011**, *3*, 19−27.
(86) Swart, M.; Gruden, M. Spinning around in Transition-Metal Chemistry. *Acc. Chem. Res.* **2016**, *49*, 2690−2697.

https://doi.org/10.1021/acs.jpca.3c02794
J. Phys. Chem. A 2023, 127, 7121−7131